2-17-2001

Semiautomated Skeletonization of the Pulmonary Arterial Tree in Micro-CT Images

Christopher C. Hanger
Medical College of Wisconsin

Steven Thomas Haworth
Medical College of Wisconsin

Robert C. Molthen
Marquette University, robert.molthen@marquette.edu

Christopher A. Dawson
Medical College of Wisconsin

Published version. Published as part of the proceedings of the conference, *Proceedings of SPIE 4321: Medical Imaging 2001: Physiology and Function from Multidimensional Images, San Diego, CA, (February 17, 2001)*, 2001: 510-516. DOI.

Semi-Automated Skeletonization of the Pulmonary Arterial Tree in Micro-CT Images

Christopher C. Hanger[a], Steven T. Haworth[b,c], Robert A. Molthen[b,c,d], and Christopher A.Dawson[b,c,d]

Departments of Anesthesia, Medical College of Wisconsin, Milwaukee, WI 53226[1]
Department of Physiology, Medical College of Wisconsin, Milwaukee, WI 53226
Department of Biomedical Engineering, Marquette University, Milwaukee, WI 53233
Department of Veterans Affairs, Zablocki VA Medical Center, Milwaukee WI 53295

ABSTRACT

We present a simple and robust approach that utilizes planar images at different angular rotations combined with unfiltered back-projection to locate the central axes of the pulmonary arterial tree. Three-dimensional points are selected interactively by the user. The computer calculates a sub-volume unfiltered back-projection orthogonal to the vector connecting the two points and centered on the first point. Because more x-rays are absorbed at the thickest portion of the vessel, in the unfiltered back-projection, the darkest pixel is assumed to be the center of the vessel. The computer replaces this point with the newly computer-calculated point. A second back-projection is calculated around the original point orthogonal to a vector connecting the newly-calculated first point and user-determined second point. The darkest pixel within the reconstruction is determined. The computer then replaces the second point with the XYZ coordinates of the darkest pixel within this second reconstruction. Following a vector based on a moving average of previously determined 3-dimensional points along the vessel's axis, the computer continues this skeletonization process until stopped by the user. The computer estimates the vessel diameter along the set of previously determined points using a method similar to the full width-half max algorithm. On all subsequent vessels, the process works the same way except that at each point, distances between the current point and all previously determined points along different vessels are determined. If the difference is less than the previously estimated diameter, the vessels are assumed to branch. This user/computer interaction continues until the vascular tree has been skeletonized.

Keywords: micro-CT imaging, 3D image processing, 3D image analysis, angiography

1. INTRODUCTION

High-resolution micro-CT scanners permit the generation of three-dimensional digital images containing extensive vascular networks such as found within the lung. Segmentation of these vascular tree structures for quantitative vascular morphometry can be difficult and time consuming. This is due, in part, to the complexity of the networks and the fact that the vessel axis has no distinguishing features in a fully reconstructed 3D image. The proposed method is based on the premise that the latter problem can be circumvented by using the original planer images at different angular rotations to locate the central axis within the contrast-enhanced vessels. This method is exemplified on images of the pulmonary arterial tree.

2. METHODS

[1] Further author information: (Send correspondence to C.H.)
Research Service 151A, Zablocki VA Medical Center, 5000 W. National Ave., Milwaukee, WI 53295
E-mail changer@mcw.edu
Phone (414) 384 2000 x41440

Medical Imaging 2001: Physiology and Function from Multidimensional Images, Chin-Tu Chen, Anne V. Clough, Editors, Proceedings of SPIE Vol. 4321 (2001) © 2001 SPIE · 1605-7422/01/$15.00

2.1. Development Environment

The algorithm runs under the Windows 95,™ Windows 98, ™ Windows 2000 ™ or Windows NT™ operating systems. The computer program is written in Microsoft Visual C++ Version 6.0. Visual C++ was chosen for its portability between different PC platforms, its rapid, user-friendly development environment and its ability to generate efficient code running under the well-understood Microsoft Windows ™ user-interface.

2.2. Image Acquisition

The lung preparation has been described previously[1]. A lung from an anesthetized rat was isolated and placed within an x-ray lucent tube on a computer driven turntable between the focal spot of an x-ray source (FeinFocus FXE100.20) and an image intensifier (North American Image Intensifier Corp.) so that it could be rotated 360°. The pulmonary arterial tree was filled with perflourooctylbromide at 20 mmHg with the airway pressure fixed at 6 mmHg. As the rat lung was rotated over 360 degrees, images were recorded using a digital CCD camera connected to a computer via a parallel RS422 interface. Each monochrome image was 512 x 512 x 8 bits. The set of 360 images was stored on the computer's hard disk.

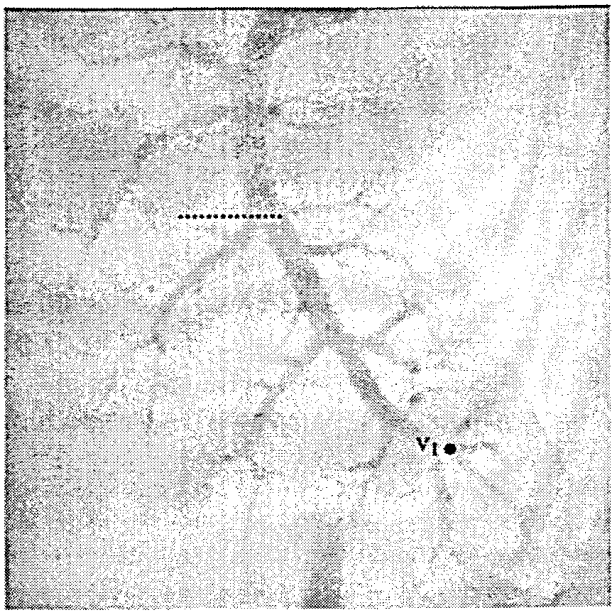

Figure 2. X-ray planar image of a left rat lung lobe. Pulmonary arteries have been filled with contrast media and appear dark. The dot v1 represents a view through the axis of a vector originating at the x-ray source and ending at the image intensifier. The dark region at the bottom center of the image is a calibration phantom near the center of rotation of the object stage.

2.3. Identification of a starting point

The software allows the user to cycle through the 360 planar images to choose a vessel segment from which to begin following the central axis. At any given view, the user identifies (mouse-clicks) a point on the vessel. The computer constructs a projection vector (v_1) through object space originating at the x-ray source and ending at the image intensifier. This vector, when viewed edge-on, appears as a point on the planar image (Fig. 2). An overhead representation of the same vector is shown (Fig. 3).

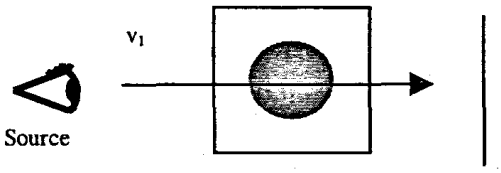

Figure 3. Schematic representation of a vector originating at the x-ray source, passing through a vessel of interest, and terminating at the image intensifier (II).

The user then chooses an image captured at a different angle of rotation. The computer superimposes v_1 , which now appears as a line, onto this rotated image (Figs. 4-5).

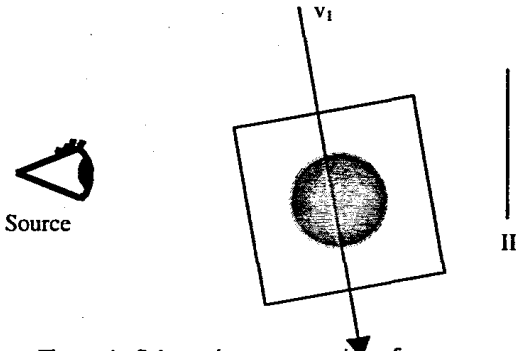

Figure 4. Schematic representation of vector v1 rotated along with object.

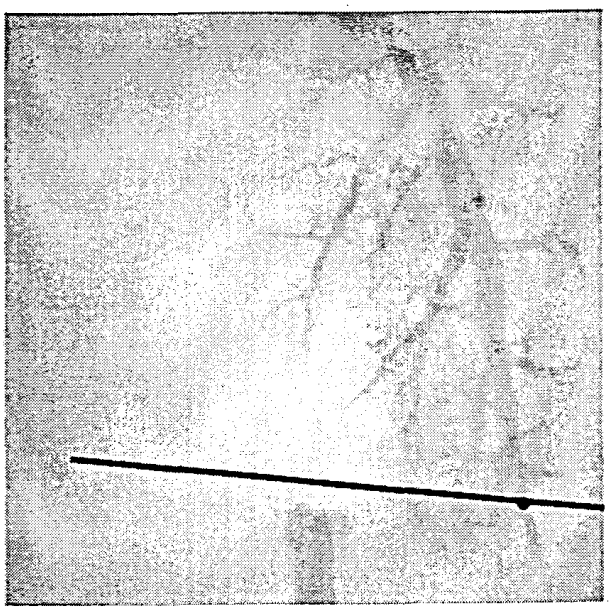

Figure 5. A different orientation of the rat lung rotated approximately 70 degrees by the user. As a different orientation of the lung image is displayed v_1 appears to rotate with the object.

The same location of the original vessel is identified (second mouse-click) where it intersects the projection of v_1. The computer constructs a second projection vector (v_2) originating at the x-ray source and ending at the image intensifier.

A three-dimensional point (p_0) is constructed at the intersection of v_1 and v_2. P_0 represents the user-initiated initial guess of the three-dimensional coordinates of the vessel center point. This process is illustrated graphically in figures 6 and 7.

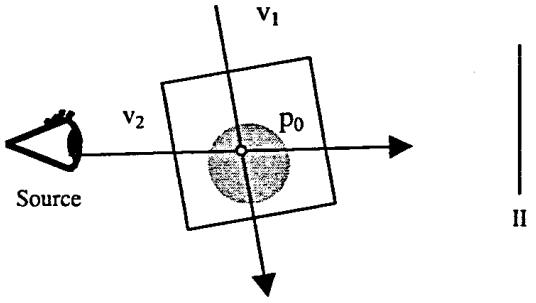

Figure 6. Schematic of vectors v_1 and v_2 and the point at their intersection, p_0.

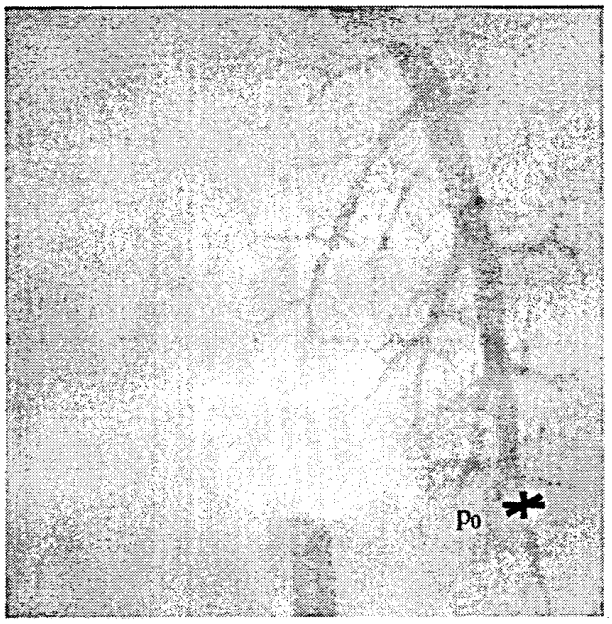

Figure 7. Three-dimensional point p_0 is superimposed on the image. Here p_0 is the intersection of vectors v_1 and v_2.

The same simultaneous vector technique is applied to create a second estimation of the vessel's center axis (p_1). The user has the ability to confirm the points' position by rotating through the set of planar images as p_0 and p_1 are continuously projected onto the images. Rotated image of vessel tree with p_0 and p_1 projected onto image is shown (Fig. 8).

2.4. Back projection

The computer calculates coefficients of a plane orthogonal to the vector passing through p_0 and p_1. Points on this orthogonal plane, centered at p_0, are back-projected in 360 orientations to create an image in which the true vessel axis lies. The back projection is carried out on a bounded subset of image-space encompassing the whole vessel cross section. The user interactively specifies the diameter of this orthogonal plane, typically approximately twice the diameter of the back-projected vessel's image.

The minimum intensity within this back projection is determined and the XYZ coordinates corresponding with minimum intensity are stored as the improved approximation to the point on the central axis (p_0*). The back projection process and 3D plot of pixel intensities are shown (Fig. 9). A key element of the method is that the unfiltered back-projection results in a single point of minimum intensity located very near the central axis of the vessel.

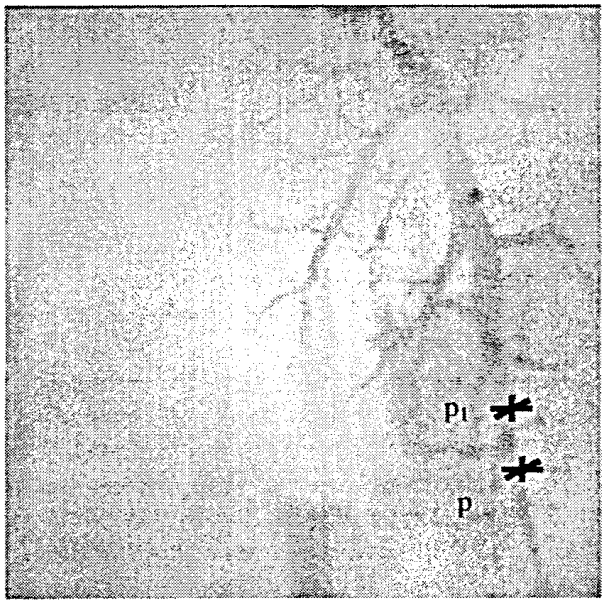

Figure 8. User has selected two three-dimensional points p0, and p1 within the vicinity of the vessel center. These points are projected onto the original planar image

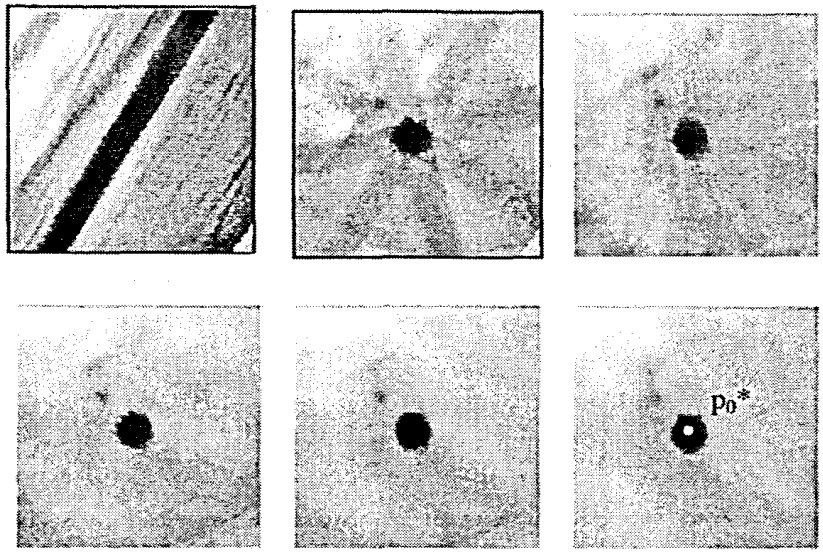

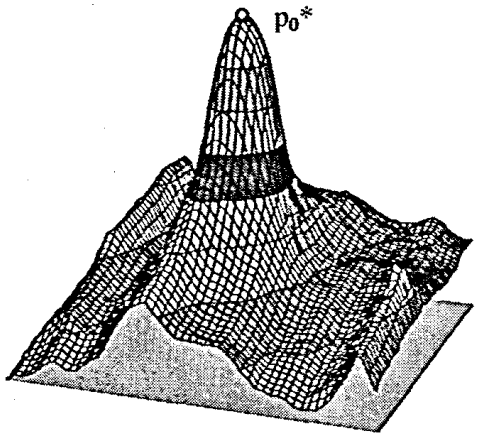

Figure 9. **Top**: Back-projections centered on p_0, lying in a plane orthogonal to vector between p_0 and p_1. **Bottom**: three-dimensional representation of pixel intensities along back projected plane after 360 projections. Pixel with minimum intensity (p_0*) is assumed to be true center of vessel.

2.4. Determining second point (p_1*)

Having computed p_0*, a vector originating at the newly determined point p_0* and ending at the original user defined point p_1 is determined. The plane orthogonal to this vector is computed and p_1* represents the XYZ coordinates of the minimum pixel within this plane.

2.5. Automated Skeletonization of entire vessel

All subsequent points (p_n*) are determined based on a moving average of vectors derived from previously determined points (p_0* - p_{n-1}*). An orthogonal plane generated around p_n and p_n* is calculated from the XYZ coordinates corresponding to the minimum intensity pixel on that plane. This skeletonization process continues in user-defined increments until stopped by the user (Fig. 10).

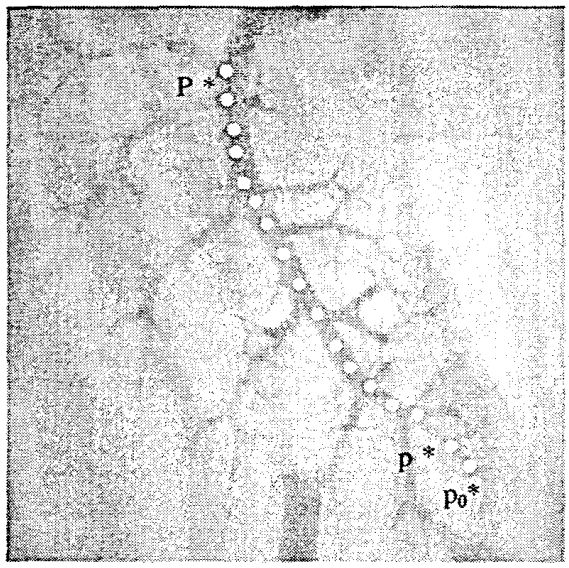

Figure 10. First vessel has been skeletonized

2.6. Diameter Estimation

The central axis of any arterial branch can be obtained in the same manner. However, to interconnect the central axes of neighboring vessels at branch points, a boundary, centered along each vessel's central axis and proportional to the vessel's diameter is required. This boundary is obtained by beginning at the central point p_n*, and working outward. All pixels within the back-projection plane are replaced with brightest pixel for every given distance. The radius of this boundary is the distance between the center point and a ring located at the level of steepest descent. This is graphically depicted in Figure 11.

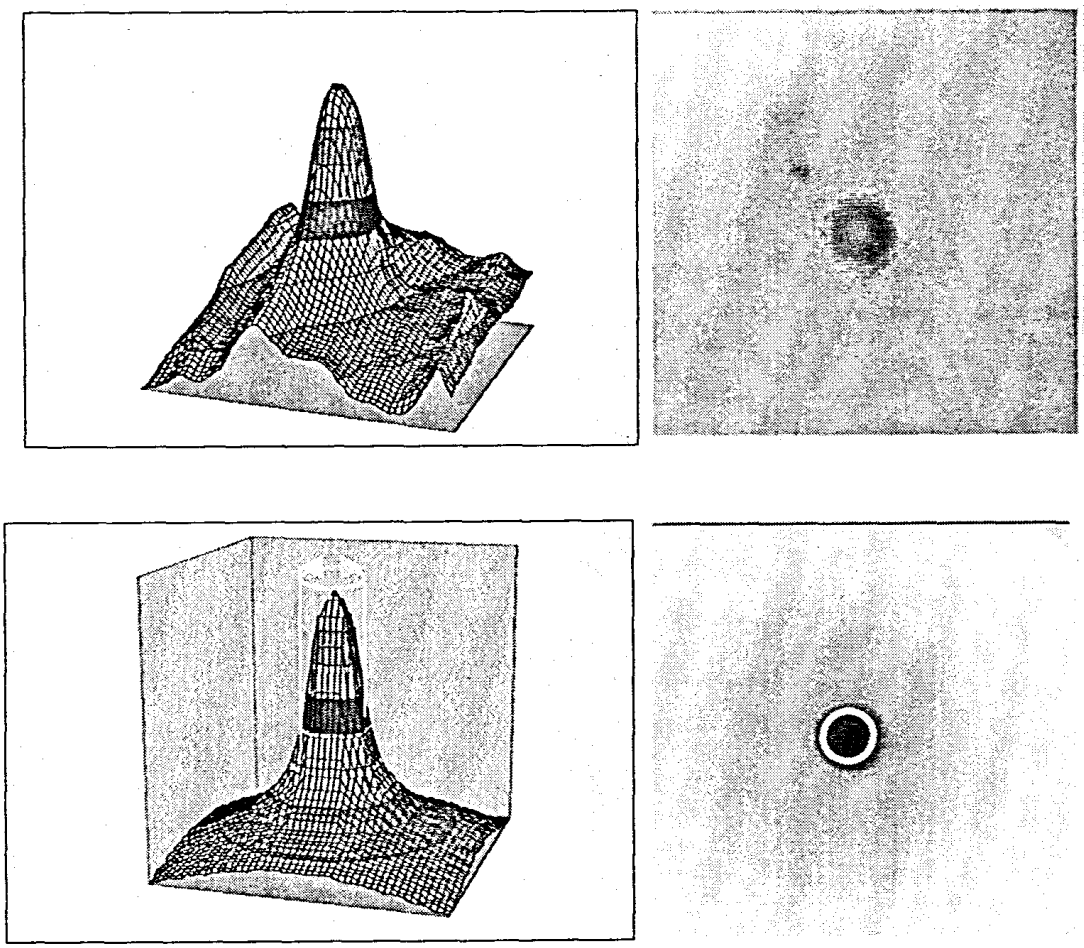

Figure 11. **Top**: Pixel intensities within back projection surrounding vessel. **Bottom**: All pixel intensities at every distance from center have been replaced with brightest pixel at that distance. The method computes boundary radius as the distance between center pixel and a ring located at the level of steepest decent.

2.7. Connecting subsequent vessels

The user identifies two 3D points (using methods described above) along a different vessel and skeletonization is once again performed. However, as each point is determined, the distances between points on all previously skeletonized vessels and the current point are determined. If this distance falls within the radius of the previously determined vessel boundary, the skeletonization process for the current vessel ends and the new point's coordinates are changed to the coordinates of the point on the existing vessel corresponding to the smallest distance. This is shown diagrammatically in Fig. 12.

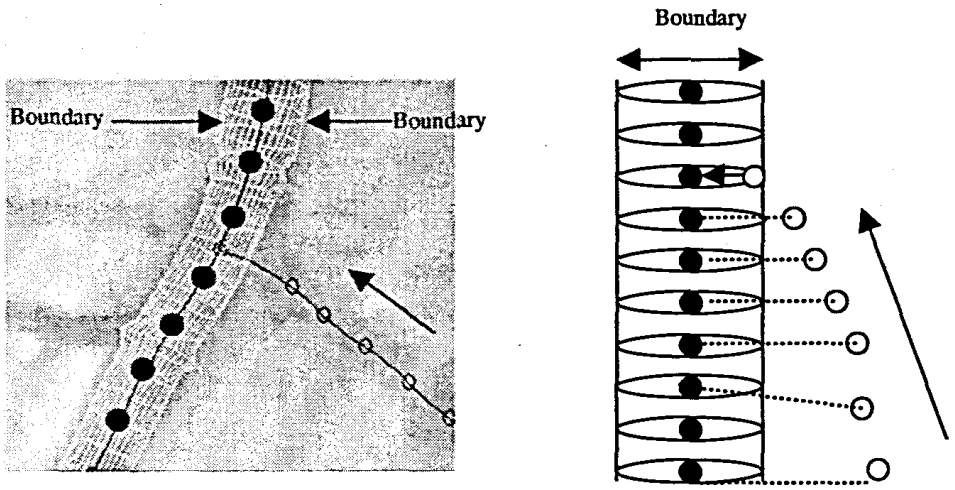

Figure 12. Connection process. New points along a vessel axis are determined (in direction of arrows). Distances between all new points (open circles), and points along central axis of previously determined vessels (filled circles) are determined. If distance (dashed line on right diagram) falls within previous vessel's boundary, this new point's position is set to the coordinates of the vessel axis point corresponding with the nearest distance.

3. Results and Discussion

Figures 13-14 shows the 3-dimensional skeleton of several orientations of a left rat lung obtained as described.

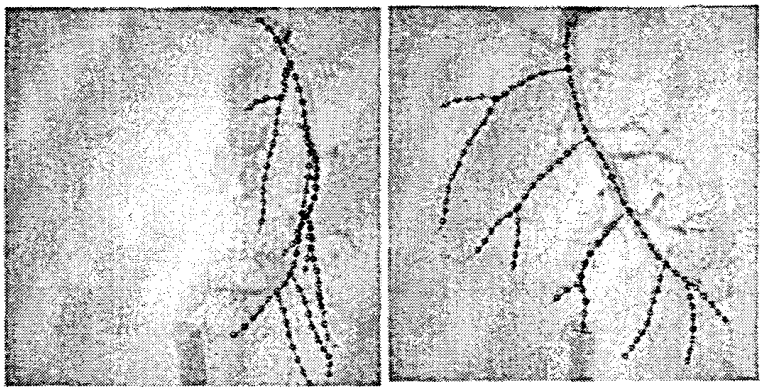

Figures 13, 14. The central axes of several skeletonized arteries of a left rat lung. Two different orientations are shown

The concept upon which this method is based is illustrated in Fig. 15 which compares the image of the vessel cross section generated by cone beam reconstruction using a Feldkamp algorithm with a vessel cross section generated by simple unfiltered backprojection. A graph of pixel intensities along a line transecting the central axis of the vessel image is also shown. While the unfiltered back projection has an easily discernable center, the fully reconstructed CT image (top) has no easily discernable center.

Many approaches have been proposed based upon, to the best of our knowledge, a completed CT reconstruction[23456]. This present approach uses raw images and unfiltered back-projection to reconstruct the central axis of vessels within the pulmonary arterial tree. Because the method does not rely on CT reconstruction, it allows a rapid "turn around time" between data acquisition and data analysis. Also, only a few images (usually < 10) captured at differing rotations are necessary to differentiate vessel from non-vessel and to identify the central pixel. Therefore, fewer image acquisitions may be necessary. This may facilitate faster data-acquisitions during studies requiring more physiologic conditions. Finally, once skeletonization information has been obtained, it can be superimposed on the full 3D reconstruction to aid in morphometric measurements.

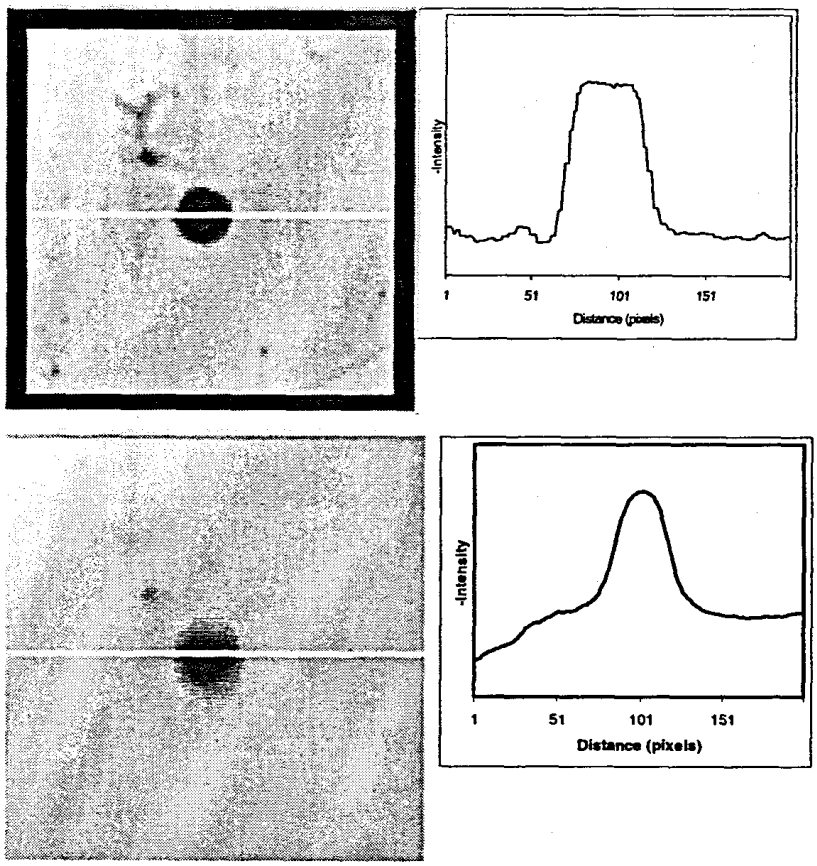

Figure 15. Comparison of vessel cross sections slices across identical location of vessel. **Top** slice taken from full CT reconstruction. **Bottom** slice from back projection.

Supported by NIH 5T32-GM08377-06, National Heart Lung and Blood Institute HL19298, the Department of Veterans Affairs, and the W.M Keck foundation

[1] Johnson, R. H., K. L. Karau. R. C. Molthen and C. A. Dawson, "Exploiting self-similarity of arterial trees to reduce the complexity of image analysis," *Proc. SPIE 3660, Physiology and Function from Multidimensional Images, 351-361, 1999.*
[2] Hoffman, E.A., I.J. Sinak, R. A. Robb, and E.L. Rittman. Noninvasive quantitative imaging of shape and volume of lungs, *J. Appl. Physiol.* 54:1414-1421, 1983.
[3] Pao, Y. C., J. T. Lu, and E. L. Rittman, Bending and twisting of an in vivo coronary artery at a bifurcation. *J. Biomech.* 25: 287-295, 1992.
[4] Rittman, E. L, Three-dimensional imaging of the heart, lungs and circulation. *Science Wash. DC* 210:273-280
[5] Rittman, E. I., and H. K. Liu, Branching pattern of pulmonary arterial tree in anesthetized dogs. *J. Biomedical Engineering* 108: 289-293 1986

PROGRESS IN BIOMEDICAL OPTICS AND IMAGING
Vol . 2, No. 26

Medical Imaging 2001

Physiology and Function from Multidimensional Images

Chin-Tu Chen
Anne V. Clough
Chairs/Editors

18–20 February 2001
San Diego, USA

Sponsored and Published by
SPIE—The International Society for Optical Engineering

Cooperating Organizations
AAPM—American Association of Physicists in Medicine
APS—American Physiological Society
FDA Center for Devices and Radiological Health (USA)
IS&T—The Society for Imaging Science and Technology
NEMA—National Electrical Manufacturers Association/Diagnostic Imaging and Therapy Systems Division (USA)
RSNA—Radiological Society of North America
SCAR—Society for Computer Applications in Radiology (USA)

Proceedings of SPIE
Volume 4321

The papers appearing in this book compose the proceedings of the technical conference cited on the cover and title page of this volume. They reflect the authors' opinions and are published as presented, in the interests of timely dissemination. Their inclusion in this publication does not necessarily constitute endorsement by the editors or by SPIE. Papers were selected by the conference program committee to be presented in oral or poster format, and were subject to review by volume editors or program committees.

Please use the following format to cite material from this book:

Author(s), "Title of paper," in *Medical Imaging 2001: Physiology and Function from Multidimensional Images*, Chin-Tu Chen, Anne V. Clough, Editors, Proceedings of SPIE Vol. 4321, page numbers (2001).

ISSN 1605-7422
ISBN 0-8194-4007-8

Published by
SPIE—The International Society for Optical Engineering
P.O. Box 10, Bellingham, Washington 98227-0010 USA
Telephone 1 360/676-3290 (Pacific Time) • Fax 1 360/647-1445
http://www.spie.org/

Printed in the United States of America.

Contents

ix *Conference Committee*

SESSION 1 PHYSIOLOGIC MODELING FROM IMAGES

1 **Multiresolution imaging of in-vivo ligand-receptor interactions** [4321-02]
P. Thévenaz, Swiss Federal Institute of Technology Lausanne; P. Millet, Hôpitaux Universitaires de Genève (Switzerland)

12 **Resolution of the spectral technique in kinetic modeling** [4321-03]
C. Kuo, B. W. Reutter, R. H. Huesman, Lawrence Berkeley National Lab. (USA)

SESSION 2 VIRTUAL ENDOSCOPY I

22 **Tracheal and central bronchial aerodynamics using virtual bronchoscopy** [4321-04]
R. M. Summers, National Institutes of Health (USA); J. R. Cebral, George Mason Univ. (USA)

32 **Virtual angioscopy in human coronary arteries with visualization of computational hemodynamics** [4321-05]
A. Wahle, S. C. Mitchell, S. D. Ramaswamy, K. B. Chandran, M. Sonka, Univ. of Iowa (USA)

44 **Virtual angioscopic visualization and analysis of coronary aneurysms using intravascular ultrasound images** [4321-06]
T. A. A. Ayeni, D. R. Holmes, R. A. Robb, Mayo Clinic and Foundation (USA)

53 **Computer-aided detection of polyps in CT colonography based on geometric features** [4321-07]
H. Yoshida, Y. Masutani, P. MacEnaney, A. H. Dachman, Univ. of Chicago (USA)

58 **Application of virtual endoscopy to patient-specific planning of endovascular surgical procedures** [4321-08]
O. Acosta, P. Haigron, Univ. de Rennes I (France); A. Lucas, Hôpital Sud Rennes (France); M.-E. Bellemare, Univ. de Rennes I (France)

SESSION 3 DYNAMIC IMAGING

70 **Carbon dioxide reactivity of tumor blood flow as measured by dynamic contrast-enhanced computed tomography: a new treatment protocol for laser thermal therapy** [4321-10]
T. G. Purdie, John P. Robarts Research Institute/Univ. of Western Ontario (Canada); M. D. Sherar, Ontario Cancer Institute (Canada) and Univ. of Toronto (Canada); A. Fenster, John P. Robarts Research Institute/Univ. of Western Ontario (Canada); T.-Y. Lee, John P. Robarts Research Institute/Univ. of Western Ontario (Canada) and St. Joseph's Health Ctr. (Canada)

81 **Interpretation of arterial velocity waveforms** [4321-11]
P. J. Yim, National Institutes of Health (USA); J. R. Cebral, R. Löhner, O. Soto, George Mason Univ. (USA); H. Marcos, P. L. Choyke, National Institutes of Health (USA)

92 **Automatic left ventricle wall motion detection in gated SPECT perfusion images** [4321-12]
M. A. Gutierrez, Univ. of São Paulo Medical School (Brazil); M. S. Rebelo, Univ. of São Paulo Medical School (Brazil) and Univ. Estadual de Campinas (Brazil); S. S. Furuie, L. Pozzo, J. C. Meneghetti, C. P. de Melo, Univ. of São Paulo Medical School (Brazil)

100 **3D quantitative visualization of altered LV wall thickening dynamics caused by coronary microembolization** [4321-13]
C. D. Eusemann, S. Mohlenkamp, E. L. Ritman, R. A. Robb, Mayo Clinic and Foundation (USA)

108 **Multimodality evaluation of ventricular function: comparison of cardiac magnetic resonance imaging, echocardiography, and planar and SPECT blood pool imaging** [4321-14]
D. H. Feiglin, A. Krol, G. M. Tillapaugh-Fay, N. M. Szeverenyi, F. D. Thomas, SUNY/Upstate Medical Univ. (USA)

SESSION 4 VIRTUAL ENDOSCOPY II: VISUALIZATION

111 **Experiments in virtual-endoscopic guidance of bronchoscopy** [4321-15]
J. P. Helferty, A. J. Sherbondy, A. P. Kiraly, J. Z. Turlington, The Pennsylvania State Univ. (USA); E. A. Hoffman, G. McLennan, Univ. of Iowa (USA); W. E. Higgins, The Pennsylvania State Univ. (USA) and Univ. of Iowa (USA)

122 **Camera motion tracking of real endoscope by using virtual endoscopy system and texture information** [4321-16]
H. Shoji, K. Mori, J. Sugiyama, Y. Suenaga, J. Toriwaki, Nagoya Univ. (Japan); H. Takabatake, Minami-ichijyo Hospital (Japan); H. Natori, Sapporo Medical Univ. (Japan)

134 **Method for detecting unobserved regions in virtual endoscopy system** [4321-17]
K. Mori, Y. Hayashi, Y. Suenaga, J. Toriwaki, Nagoya Univ. (Japan); J. Hasegawa, Chukyo Univ. (Japan); K. Katada, Fujita Health Univ. (Japan)

146 **Evaluation of virtual endoscopy for exploratory navigation inside vascular structures** [4321-18]
P. Haigron, Univ. de Rennes I (France); A. Lucas, Hôpital Sud Rennes (France); L. Quiniou, A. Mom, Univ. de Rennes II (France)

155 **Gesture analysis and immersive visualization for virtual endoscopy** [4321-19]
K.-H. Englmeier, M. Siebert, National Research Ctr. for Environment and Health (Germany); R. Brüning, J. Scheidler, M. Reiser, Klinikum Großhadern/Ludwig-Maximilians-Univ. München (Germany)

SESSION 5 NEW DEVELOPMENTS IN FUNCTIONAL IMAGING

163 **Ultrasound images of implanted tumors in nude mice using Sono-CT correlated with MRI appearance** [4321-20]
M. T. Freedman, A. Sarcone, K. F. Pirollo, C.-S. Lin, E. Chang, Georgetown Univ. Medical Ctr. (USA)

168 **Comparison of near-infrared spectroscopy with CT cerebral blood flow measurements in newborn piglets** [4321-21]
D. W. Brown, St. Joseph's Health Ctr. (Canada), London Health Science Ctr. (Canada), and Univ. of Western Ontario (Canada); P. A. Picot, St. Joseph's Health Ctr. (Canada) and Univ. of Western Ontario (Canada); R. Springett, D. T. Delpy, Univ. College London (UK); T.-Y. Lee, St. Joseph's Health Ctr. (Canada), London Health Science Ctr. (Canada), and Univ. of Western Ontario (Canada)

177 **New methods for computational fluid dynamics modeling of carotid artery from magnetic resonance angiography** [4321-22]
J. R. Cebral, George Mason Univ. (USA); P. J. Yim, National Institutes of Health (USA); R. Löhner, O. Soto, George Mason Univ. (USA); H. Marcos, P. L. Choyke, National Institutes of Health (USA)

188 **Neuronal current imaging using MRI: a feasibility study** [4321-23]
N. Petridou, J. Bodurka, National Institutes Health (USA); M. H. Loew, George Washington Univ. (USA); P. A. Bandettini, National Institutes Health (USA)

195 **Strain-encoded (SENC) harmonic phase imaging for fast magnetic resonance elastography** [4321-24]
N. F. Osman, Johns Hopkins Univ. School of Medicine (USA)

SESSION 6 LUNG IMAGING

204 **Lung lobe segmentation by graph search with 3D shape constraints** [4321-25]
L. Zhang, E. A. Hoffman, J. M. Reinhardt, Univ. of Iowa (USA)

216 **Fast pulmonary contour extraction in x-ray CT images: a methodology and quality assessment** [4321-26]
A. F. Silva, Univ. of Aveiro (Portugal); J. S. Silva, Univ. of Coimbra (Portugal); B. S. Santos, Univ. of Aveiro (Portugal); C. Ferreira, Univ. of Aveiro (Portugal) and Univ. of Lisbon (Portugal)

225 **Changes of air-tissue ratio evaluated by EBCT after cardiopulmonary resuscitation (CPR): validation in swine** [4321-27]
W. A. Recheis, A. H. Schuster, A. Kleinsasser, A. Löckinger, C. Hoermann, D. zur Nedden, Univ. Hospital Innsbruck (Austria)

234 **Evaluation and application of 3D lung warping and registration model using HRCT images** [4321-28]
L. Fan, Siemens Corporate Research, Inc. (USA); C. W. Chen, Univ. of Missouri/Columbia (USA); J. M. Reinhardt, Univ. of Iowa (USA) and Univ. of Iowa College of Medicine (USA); E. A. Hoffman, Univ. of Iowa College of Medicine (USA) and Univ. of Iowa (USA)

244 **New approach to diagnosis of pulmonary embolism using multislice CT** [4321-29]
M. U. Niethammer, Siemens AG (Germany); U. J. Schoepf, Univ. of Munich (Germany); J. E. Wildberger, Aachen Univ. of Technology (Germany); E. Klotz, H. Fichte, S. Schaller, Siemens AG (Germany)

254 **Improved algorithm for computerized detection and quantification of pulmonary emphysema at high-resolution computed tomography (HRCT)** [4321-30]
U. Tylén, Göteborg Univ./Sahlgrenska Univ. Hospital (Sweden); O. Friman, M. Borga, Linköping Univ. Hospital (Sweden); J.-E Angelhed, Göteborg Univ./Sahlgrenska Univ. Hospital (Sweden)

SESSION 7 IMAGING OF THE VASCULATURE

263 **Voxel-coding method for quantification of vascular structure from 3D images** [4321-31]
H. Soltanian-Zadeh, Univ. of Tehran (Iran), School of Intelligent Systems (Iran), and Henry Ford Health System (USA); A. Shahrokni, Univ. of Tehran (Iran) and School of Intelligent Systems (Iran); R. A. Zoroofi, Univ. of Tehran (Iran)

271 **Analysis of the morphology and structure of vessel systems using skeletonization** [4321-32]
D. Selle, H.-O. Peitgen, MeVis/Univ. of Bremen (Germany)

282 **Pulmonary arterial remodeling revealed by microfocal x-ray tomography** [4321-33]
K. L. Karau, Marquette Univ. (USA) and Medical College of Wisconsin (USA); R. C. Molthen, R. H. Johnson, Marquette Univ. (USA) and Zablocki Veterans Affairs Medical Ctr. (USA); A. H. Dhyani, Marquette Univ. (USA); S. T. Haworth, Medical College of Wisconsin (USA); C. A. Dawson, Marquette Univ. (USA), Medical College of Wisconsin (USA), and Zablocki Veterans Affairs Medical Ctr. (USA)

288 **Dynamic three-dimensional model of the coronary circulation** [4321-34]
G. C. Lehmann, John P. Robarts Research Institute/Univ. of Western Ontario (Canada); D. G. Gobbi, John P. Robarts Research Institute/Univ. of Western Ontario (Canada) and Univ. of Western Ontario (Canada); A. J. Dick, London Health Sciences Ctr. (Canada); Y. P. Starreveld, John P. Robarts Research Institute/Univ. of Western Ontario (Canada), Univ. of Western Ontario (Canada), and London Health Sciences Ctr. (Canada); M. Quantz, London Health Sciences Ctr. (Canada); D. W. Holdsworth, M. Drangova, John P. Robarts Research Institute/Univ. of Western Ontario (Canada) and Univ. of Western Ontario (Canada)

298 **X-ray measurement of regional blood flow distribution using radiopaque contrast medium: influence of gravity** [4321-35]
A. V. Clough, Marquette Univ. (USA); S. T. Haworth, D. T. Roerig, C. C. Hanger, Medical College of Wisconsin (USA) and Zablocki Veterans Administration Medical Ctr. (USA); C. A. Dawson, Marquette Univ. (USA), Medical College of Wisconsin (USA), and Zablocki Veterans Affairs Medical Ctr. (USA)

305 **Doppler blood velocity assessment based on image analysis of video-tape-recorded image data** [4321-36]
J. Tschirren, R. M. Lauer, M. Sonka, Univ. of Iowa (USA)

SESSION 8 FUNCTIONAL MAGNETIC RESONANCE IMAGING

312 **Blind source separation (BSS) for fMRI analysis** [4321-37]
T. Lei, J. K. Udupa, Univ. of Pennsylvania (USA)

321 **Dynamics of fMRI signals during human brain activations to a stimulus** [4321-38]
H. Liu, T. Kato, C. Neves, Univ. of Minnesota/Twin Cities (USA)

327 **Analysis of event-related fMRI using a nonlinear regression self-organizing map neural network** [4321-39]
S. G. Erberich, M. Liebert, K. Willmes, A. Thron, Univ. Hospital/Aachen Univ. of Technology (Germany); W. Oberschelp, Aachen Univ. of Technology (Germany)

336 **Optimized knowledge-based motion correction of fMRI time series using parallel algorithms** [4321-40]
T. Schmidt, S. G. Erberich, M. Hoppe, C. Jansen, A. Thron, Univ. Hospital/Aachen Univ. of Technology (Germany); W. Oberschelp, Aachen Univ. of Technology (Germany)

348 **Using fMRI to guide neurosurgery in a combined 1.5-Tesla MR operating room** [4321-41]
H. Liu, W. A. Hall, A. J. Martin, R. E. Maxwell, C. L. Truwit, Univ. of Minnesota/Twin Cities (USA)

SESSION 9 BRAIN IMAGING

354 **MR mapping of temperature and perfusion for hyperthermia therapy** [4321-42]
W. Wlodarczyk, J. Vlad, T. Lange, P. Wust, R. Felix, Virchow Klinikum/Humboldt-Univ. zu Berlin (Germany)

362 **Multimodality localization of epileptic foci** [4321-43]
M. Desco, J. Pascau, Hospital General Universitario Gregorio Marañón (Spain); M. A. Pozo, Univ. Complutense de Madrid (Spain); A. Santos, Univ. Politécnica de Madrid (Spain); S. Reig, J. D. Gispert, P. García-Barreno, Hospital General Universitario Gregorio Marañón (Spain)

371 **Using intraoperative MRI to assess bleeding** [4321-44]
H. Liu, W. A. Hall, A. J. Martin, C. L. Truwit, Univ. of Minnesota/Twin Cities (USA)

375 **New method for quantitative analysis of multiple scelerosis using MR images** [4321-45]
D. Chen, W. Huang, C. Christodoulou, L. Li, H. Qian, L. Krupp, Z. Liang, SUNY/Stony Brook (USA)

381 **Efficient MR-based screening method for Alzheimer's disease** [4321-46]
H. Liu, T. Kato, D. Knopman, Univ. of Minnesota/Twin Cities (USA)

387 **Tissue characterization in cerebral ischemia using multiparameter MRI** [4321-47]
H. Soltanian-Zadeh, Henry Ford Health System (USA) and Univ. of Tehran (Iran); R. Hammoud, Henry Ford Health System (USA); M. A. Jacobs, Henry Ford Health System (USA) and Johns Hopkins Univ. (USA); S. C. Patel, P. D. Mitsias, M. Pasnoor, R. Knight, Z. G. Zheng, M. Lu, M. Chopp, Henry Ford Health System (USA)

POSTER SESSION

399 **Brain miner: a 3D visual interface for the investigation of functional relationships in the brain** [4321-49]
T. F. Welsh, K. D. Mueller, W. Zhu, J. R. Meade, SUNY/Stony Brook (USA); N. Volkow, Brookhaven National Lab. (USA)

404 **Evidential value of postmortem MRI in forensic pathology** [4321-50]
W. Schweitzer, Univ. of Bern (Switzerland); M. E. Schaepman, Univ. of Zürich (Switzerland); M. Ith, K. Brügger, M. J. Thali, T. Dörnhöfer, K. Tiefenthaler, E. Scheurer, P. Vock, C. Boesch, R. Dirnhofer, Univ. of Bern (Switzerland)

409 **Regional deconvolution method for partial volume correction in brain PET** [4321-51]
H. Rusinek, New York Univ. School of Medicine (USA); W.-H. Tsui, New York Univ. School of Medicine (USA) and Nathan S. Kline Institute for Psychiatric Research (USA); M. J. de Leon, New York Univ. School of Medicine (USA)

419 **Biased anisotropic diffusion method for PET image segmentation** [4321-52]
H.-D. Lin, H.-Y. Wang, Y.-C. Hu, K.-P. Lin, Chung-Yuan Christian Univ. (Taiwan) C.-L. Yu, L.-C. Wu, R.-S. Liu, Taipei Veterens General Hospital (Taiwan)

427 **Quantitative analysis and visualization of the endocardial and epicardial walls using gated SPECT images** [4321-53]
S.-M. Choi, Y.-K. Lee, M.-H. Kim, Ewha Woman's Univ. (Korea)

436 **Almost automatic method for reconstruction 3D geometric model of the left ventricle from 3D + 1D precordial echocardiogram** [4321-54]
Y.-T. Ching, Y.-H. Liu, C.-L. Chang, National Chiao Tung Univ. (Taiwan); J. S. J. Chen, National Taiwan Univ.

442 **Applying focal spot unsharpness to resolve ambiguity in 3D reconstruction from biplane coronary angiograms** [4321-55]
C. H. Slump, M. Schrijver, Univ. of Twente (Netherlands); C. J. Storm, Medisch Ctr. Rijnmond-Zuid (Netherlands)

450 **Tracking points in sequence of arteries in cineangiography** [4321-56]
A. C. dos Santos, S. S. Furuie, J. C. B. Figueiredo, Univ. of São Paulo Medical School (Brazil)

458 **Myocardial fractional flow reserve: a biplane angiocardiographic alternative to the pressure gradient method** [4321-57]
M. Schrijver, Univ. of Twente (Netherlands) and Mayo Clinic and Foundation (USA); C. H. Slump, Univ. of Twente (Netherlands); C. J. Storm, Medisch Ctr. Rijnmond-Zuid (Netherlands)

467 **Correlation-timing-based erythrocyte velocity measurement using CCD imagery** [4321-58]
W. J. O'Reilly, Mercury Computer Systems, Inc. (USA) and Medical College of Wisconsin (USA); A. G. Hudetz, Medical College of Wisconsin (USA)

475 **Hybrid optical flow and segmentation technique for LV motion detection** [4321-61]
T. Macan, S. Lončarić, Univ. of Zagreb (Croatia)

483 **Interactive electronic biopsy for 3D virtual colonscopy** [4321-62]
M. Wan, Boeing Co. (USA); F. Dachille, K. Kreeger, S. Lakare, M. Sato, A. E. Kaufman, M. Wax, Z. Liang, SUNY/Stony Brook (USA)

489 **CT colonscopy: experience of 100 cases using volumetric rendering** [4321-63]
K. D. Hopper, M. Khandelwal, C. Thompson, The Pennsylvania State Univ. (USA)

495 **Paranasal sinus surgery planning using CT virtual reality** [4321-64]
K. D. Hopper, The Pennsylvania State Univ. (USA)

500 **Interactive navigation for PC-based virtual colonscopy** [4321-65]
F. Dachille, K. Kreeger, M. Wax, A. E. Kaufman, Z. Liang, SUNY/Stony Brook (USA)

505 **Transition zone: effect on image quality of CT virtual reality** [4321-66]
K. D. Hopper, The Pennsylvania State Univ. (USA)

510 **Semiautomated skeletonization of the pulmonary arterial tree in micro-CT images** [4321-67]
C. C. Hanger, Medical College of Wisconsin (USA); S. T. Haworth, Medical College of Wisconsin (USA) and Marquette Univ. (USA); R. C. Molthen, C. A. Dawson, Medical College of Wisconsin (USA), Marquette Univ. (USA), and Zablocki Veterens Affairs Medical Ctr. (USA)

517 *Addendum*
519 *Author Index*